Effect of nano-particle size on product distribution and kinetic parameters of Fe/Cu/La catalyst in Fischer-Tropsch synthesis

Ali Nakhaei Pour[1,2*],   Mohammad Reza Housaindokht[1],   Sayyed Faramarz Tayyari[1],   Jamshid Zarkesh[2]

1. Department of Chemistry, Ferdowsi University of Mashhad, P. O. Box 91775-1436, Mashhad, Iran;
2. Research Institute of Petroleum Industry of National Iranian Oil Company, P. O. Box 14665-137, Tehran, Iran

[Manuscript received July 12, 2009; revised August 24, 2009]

Abstract
Effects of nano-particle size on hydrocarbon production rates and distributions for precipitated Fe/Cu/La catalysts in Fischer-Tropsch synthesis were investigated. Nano-structured iron catalyst was prepared by micro-emulsion method. The concept of two superimposed Anderson-Schulz-Flory (ASF) distributions has been applied for the representation of the effects of reaction conditions and nano-particles size on kinetics parameters and product distributions. These results reveal that by reducing the particle size of catalyst, the break in ASF distributions was decreased. Also useful different kinetics equations for synthesis of C_3 to C_9 and C_{10} to C_{22} were determined by using α_1 and α_2 chain growth probabilities.

Key words
chain length distribution; Fischer-Tropsch synthesis; iron-based catalyst; nano-particle size

1. Introduction

The Fischer-Tropsch (FT) synthesis converts synthesis gas in a product spectrum consisting of a complex multicomponent mixture of linear and branched hydrocarbons and oxygenated products [1−3]. In 1946, Herington reported that a model of stepwise addition of single-carbon units could predict the fraction of product at each carbon number [4,5]. The same formulation was rediscovered by Anderson et al. in 1951 and named the Anderson-Schulz-Flory (ASF) distribution [1,5]. In the ASF model, the formation of hydrocarbon chains was assumed as a stepwise polymerization procedure and the chain growth probability was assumed to be independent of the carbon number. However, in practice, "ideal" molecular weight distributions were never observed [6−10]. In extensive studies of six iron catalysts in a German pilot plant in 1943, the "Schwarzheide tests", an increase or "break" in the slope of Schulz-Flory plots was observed at carbon number of about 10. This phenomenon received little further attention until recently, when several investigators reported the same effect under a variety of conditions, suggesting that it may be a rather general phenomenon. Pichler et al. [11] for the first time reported the deviations of experimental results from the ASF distribution. The usual deviations of the distribution of the linear hydrocarbons are a relatively higher

selectivity to methane, a relatively lower selectivity to ethane, and an increase in the chain growth probability with increasing carbon number in comparison to the ideal ASF distribution. Heat and mass-transfer limitations and hydrogenolytic cleavage of the 1-olefins in secondary reactions, are reported in the literature as possible reasons for high methane yields [12–14]. Lower selectivity to ethane finding is attributed to another secondary reaction of the olefins, namely incorporation into the polymer by initiating a new chain [14,15].

Several different explanations about the cause of these deviations have been proposed [16−19]. Madon and Taylor [17] interpreted this bimodal distribution by differently structured sites causing different growth probabilities. Gaube et al. [18,19] supposed that in the case of alkali promoted iron catalysts not all active sites are influenced by alkali. Therefore the distribution of higher growth probably was attributed to products formed on promoted active sites while the other part of the product is formed on un-promoted sites with a similar growth probability as evaluated for the product formed on un-promoted iron catalysts. However, the work of Dictor and Bell [13] indicated that two chain growth probabilities exist even on catalysts not promoted by potassium. Satterfield et al. [20−22] interpreted the deviations from the standard ASF distribution by the superposition of two ASF distributions. They suspected the existence of two sorts of sites for the

---

chain growth on the catalyst surface and, therefore, proposed that each site might individually yield the ideal ASF distribution with different chain growth probabilities. Patzlaff et al. [23] indicated that chain length distributions of products obtained on cobalt catalysts are slightly modified by secondary chain growth of readsorbed alkenes and hydrogenolysis of hydrocarbons. In our previous works [24–28], the effects of the zeolite and/or alkali promoters on product distributions of iron catalyst were studied.

Recent studies showed those nanosized iron particles were considered essential to achieve high FTS activity [29−33]. The method of catalyst preparation plays an important role in the physical properties and catalytic performance of the catalysts [31−33]. In the last years, it has been generalized the use of microemulsions as nanoreactors in order to synthesize nanoparticles of controlled size displaying a homogeneous distribution of both elements throughout the solid [31,32]. A microemulsion is an optically transparent and thermodynamically stable dispersion of a water phase into an organic phase stabilized by a surfactant [33]. If the minority phase is the aqueous one, then reversed micelles are obtained. Amongst advantages such as rendering nanosized particles, usually displaying high surface area and low microporosity, microemulsion is an ideal technique for the preparation of materials containing two (or more) metallic or oxide phases [31]. The different species (oxide precursors) are homogeneously mixed within the micelles, therefore rendering solids displaying high internal homogeneity and an optimal interaction between its constituents [31,32].

In this experiment, the hydrocarbon production rates and its carbon number distribution of conventional and nanosize lanthanum promoted iron catalysts in Fischer-Tropsch syntheses were studied. The concept of Anderson-Schulz-Flory (ASF) distribution with double chain growth probabilities was used for evaluation of experimental data and establish two kinetics equations for hydrocarbons production rates.

2. Data analysis

As discussed above, the hydrocarbon products of the Fischer-Tropsch synthesis are generally taken to follow the ASF distribution. For carbon number i, the mole fraction of product x_i as determined by a single chain growth probability α, is given by:

$$x_i = (1-\alpha)\alpha^{i-1} \tag{1}$$

In this work, the carbon number distribution of Fischer-Tropsch products on conventional and nano-size precipitated iron catalysts was studied by use of a modified Anderson-Schulz-Flory (ASF) distribution with two chain growth probabilities. This method was proposed by Donnelly et al. [22] and is used to characterize the carbon number distribution of Fischer-Tropsch synthesis where independent ASF distributions with different chain growth probabilities are superimposed.

$$x_i = A\alpha_1^{i-1} + B\alpha_2^{i-1} \tag{2}$$

Instead, we note that at the break point on ASF diagram, the contributions of each term in Eq. (2) are equal.

$$A\alpha_1^{i-1} = B\alpha_2^{i-1} \quad i = \xi \tag{3}$$

At break point, i is illustrated as ξ and necessarily not an integral carbon number. In this model A and B were not assumed to correspond directly to the fractions of products produced from α_1 and α_2, respectively. Instead the sum of the mole fractions over all carbon numbers is unity:

$$\sum_{i=1}^{\infty} x_i = \sum_{i=1}^{\infty} [A\alpha_1^{(i-1)} + B\alpha_2^{(i-1)}] = 1 \tag{4}$$

Methane and ethane do not obey the ASF equation and after removing C_1 and C_2 products to fit theoretical distributions to data Equation (4) leads to:

$$\sum_{i=3}^{\infty} x_i = \sum_{i=1}^{\infty} \left[A\alpha_1^{(i-1)} + B\alpha_2^{(i-1)} \right] - A(1+\alpha_1) - \\ B(1+\alpha_2) = 1 - x_1^{\text{exp}} - x_2^{\text{exp}} \tag{5}$$

Therefore, the determination of growth probabilities of the bimodal ASF distribution is based on hydrocarbons with carbon numbers $i>2$. The bimodal distribution is characterized by two growth probabilities (α_1 and α_2) and the point of intersection ξ of both ASF distributions. The mathematical procedure given by Donnelly et al. [22] arrives at

$$A = \left(1 - x_1^{\text{exp}} - x_2^{\text{exp}}\right) \left[\frac{\alpha_2^1}{1-\alpha_1} + \left(\frac{\alpha_1}{\alpha_2}\right)^{\xi-1} \cdot \left(\frac{\alpha_2^2}{1-\alpha_2}\right) \right]^{-1} \tag{6}$$

and finally

$$\frac{x_i}{1 - x_1^{\text{exp}} - x_2^{\text{exp}}} = \left[\alpha_1^{i-1} + \left(\frac{\alpha_1}{\alpha_2}\right)^{\xi-1} \cdot \alpha_2^{i-1} \right] \cdot \\ \left[\frac{\alpha_1^2}{1-\alpha_1} + \left(\frac{\alpha_1}{\alpha_2}\right)^{\xi-1} \cdot \left(\frac{\alpha_2^2}{1-\alpha_2}\right) \right]^{-1} \tag{7}$$

The three parameters α_1, α_2 and ξ are evaluated by minimizing the least squares:

$$\Phi = \sum_{i=3}^{I} \left(\ln x_1 - \ln x_l^{\text{exp}} \right)^2 = \min \tag{8}$$

in which I is the upper limit of experimental data. The advantage of Donnelly method is its independence of this upper limit I. However, the intersection point ξ is a formal parameter without any physicochemical relevance.

3. Kinetics

The hydrocarbon production rates on an alkali-promoted iron catalyst have been correlated empirically by Dictor and Bell [13] as power-law kinetics:

$$R_{\text{C}_i} = k_i P_{\text{H}_2}^a P_{\text{CO}}^b \tag{9}$$

The formation rate of the hydrocarbons appeared to increase with P_{H_2}. Assuming ASF for the distribution of the

small-chain hydrocarbons, the chain growth probability α appeared to increase with increasing CO pressure and decreasing H_2 pressure. The hydrocarbon production rates could be calculated using [13,34]:

$$R_{C_i} = R_{C_1} \alpha^{i-1} \qquad (10)$$

Where, R_{Ci} is the molar rate of hydrocarbons production with i carbon atoms and R_{C_1} is the apparent rate of synthesis for $i = 1$ but does not necessarily represent the rate of methane formation. In this study, we consider C_3 production rate as R_{C_1} and α_1 as α for $i = 4$ to 9 and C_{10} production rate as R_{C_1} using the α_2 for $i = 11$ to 22 and compared calculated hydrocarbons production rates with experimental results. The dependence of R_{Ci} on temperature and H_2 and CO partial pressures can now be expressed through R_{C_1} and α. The dependence of the chain growth probability factor α on CO and H_2 pressures has been correlated empirically [13]. α increases with increasing the CO pressure and decreases with increase in H_2 pressure. From its definition [13,34,35], we can relate α to the ratio of the rates of chain propagation, r_p and chain termination, r_t.

$$\frac{1-\alpha}{\alpha} = \frac{r_p}{r_t} \qquad (11)$$

Based on Dictor and Bell [13] results we presume that the right-hand side of Eq. (11) will be a function of the partial pressures of H_2 and CO and temperature. The relative value of the reaction activation barriers for chain growth and termination steps in the FTS reaction can be determined using Arrhenius theory for evaluation of temperature dependency of α, based on Yang et al. method [35]:

$$r_p = A_p \exp\left(\frac{-E_p}{RT}\right) \qquad (12)$$

$$r_t = A_t \exp\left(\frac{-E_t}{RT}\right) \qquad (13)$$

E_p and E_t are activation energies for propagation and termination reactions, respectively. With the introduction of Eqs. (12) and (13) into Eq. (11) we obtain:

$$\frac{1-\alpha}{\alpha} = \frac{A_t}{A_p} \exp\left(\frac{E_p - E_t}{RT}\right) \qquad (14)$$

then, when Eq. (14) is converted to logarithmic form we have:

$$\ln\frac{1-\alpha}{\alpha} = \ln\frac{A_t}{A_p} + \left(\frac{E_p - E_t}{RT}\right) \qquad (15)$$

Eq. (15) predicts a linear plot of $\ln[(1-\alpha)/\alpha]$ versus $1/T$ with slope $(E_p-E_t)/R$ and intercept $\ln A_t/A_p$.

4. Experimental

4.1. Catalyst preparation

A Fe-Cu-La conventional catalyst was prepared by co-precipitation of Fe and Cu nitrates at a constant pH to form porous Fe-Cu oxyhydroxide powders that were promoted by impregnation with $La(NO_3)_3$ precursor after treatment in air, as described previously [24–27].

The Fe-Cu-La nano-catalyst precursors were prepared by co-precipitation in a water-in-oil microemulsion as described previously [30]. Briefly, a water solution of metal precursors, $Fe(NO_3)_3 \cdot 9H_2O$ (Fluka, 98%–100%) and/or $Cu(NO_3)_2 \cdot 4H_2O$ (Fluka, purum, >97%), was added to a mixture of an oil phase containing 1-butanol (Aldrich, >99%) and chloroform (Aldrich, >99%) with respective ratio of 60 to 40 and sodium dodecyl sulfate (SDS) as surfactant. The resulting mixture had the following composition: 10wt.% of aqueous phase, 70wt.% of oil phase and 20wt.% of surfactant. After stirring, a transparent mixture, stable for at least 24 h, was obtained. A similar microemulsion containing NH_4OH (28.0%–30.0%) in the aqueous phase was used as the precipitating agent. The resulting mixture was let to decant overnight. The solid was recovered by centrifugation and washed thoroughly with distilled water and ethanol. Finally, the sample was dried overnight at 393 K and subsequently calcined in air at 773 K for 6 h. Lanthanum promoter was added by wet impregnation with $La(NO_3)_3$ precursor and the sample was set to the optimal value after treatment in air as described previously [24–28]. The promoted catalysts were dried at 383 K for 16 h and calcined at 773 K for 3 h in air. The catalyst compositions were designated in terms of the atomic ratios as: 100Fe/5.64Cu/2La.

All samples were pressed into pellets and then crushed and sieved to obtain $250-300$ μm particles which have been proved to be a compromising particle size safe for neglecting intraparticle transfer limitations and promising easy operations to the reactor during the experiment.

4.2. Catalyst characterization

N_2 physisorption was carried out with surface area and pore size analyzers (Micrometertics ASAP 2010 Instruments) at 77 K to determine the BET surface area and pore size distribution of the oxide precursors. Before the measurements, the samples were degassed at 393 K for 3 h. Both the pore volume and the average pore diameter were calculated by Barret-Joyner-Hallender (BJH) method from the desorption isotherm.

The H_2-TPD experiments were performed by means of the temperature programmed desorption (TPD) of H_2 using 0.5 g of catalyst in a quartz reactor. The reactor was operated in a temperature range of 300 to 1100 K at a linear heating rate of 5 K/min while Ar was used as a carrier gas. A thermal conductivity detector was used to measure the H_2 desorbed in the TPD quantitatively. The catalyst was first reduced with H_2 at 673 K and 0.1 MPa for 11 h. Then the sample was heated in Ar from 323 to 673 K, held at 673 K until the baseline leveled off (ensuring complete removal of adsorbed species on the reduced catalyst surface has been achieved), and finally cooled to 323 K for TPD tests. In the subsequent steps, H_2 adsorption on the catalyst was performed at 323 K for 30 min, and then the sample was purged with Ar in order that weakly adsorbed species could be removed until the baseline leveled

off. Following this, H_2-TPD was carried out while the temperature was increased to 1050 K. H_2 chemisorptions uptakes were determined by integrating the area of H_2-TPD curves as compared to the known amounts of H_2 gas passed through the TCD.

4.3. Catalytic performance

A detailed description of the experimental setup and procedures has been provided elsewhere [24–28]. The catalyst samples (the 1.5 g catalysts diluted with 4 g quartz, 250–300 μm) were activated by a 5%(v/v) H_2/N_2 gas mixture with space velocity of 15.1 nl·h^{-1}·g$_{Fe}^{-1}$ at 0.1 MPa by increasing temperature from ambient to 673 K at 5 K/min, then maintained for one hour and subsequently reduced to 543 K. The activation is followed by the passage of the synthesis gas stream with $H_2/CO = 1$ and space velocity of 3.07 nl·h^{-1}·g$_{Fe}^{-1}$ for 24 h in 0.1 MPa and 543 K before setting the actual reaction temperature and pressure. After activation, the catalyst activity tests were performed at 563 K, 1.7 MPa, $H_2/CO = 1$ and space velocity of 4.9 nl·h^{-1}·g$_{Fe}^{-1}$. For evaluation of the results in various reaction conditions, reaction temperature and H_2/CO partial pressure ratios in feed were varied between 543 and 603 K and 0.5 to 2 (with total of 1.7 MPa), respectively.

The products were analyzed by means of three gas chromatographs, a Shimadzu 4C gas chromatograph equipped with two subsequent connected packed columns: Porapak Q and Molecular Sieve 5A, and a thermal conductivity detector (TCD) with argon which was used as a carrier gas for hydrogen analysis. A Varian CP 3800 with a chromosorb column and a thermal conductivity detector (TCD) were used for CO, CO_2, CH_4, and other non-condensable gases. A Varian CP 3800 with a Petrocol^{Tm} DH100 fused silica capillary column and a flame ionization detector (FID) were used for organic liquid products so that a complete product distribution could be provided.

5. Results

5.1. Textural structure of the catalysts

BET surface area, pore volume and pore diameter of the catalysts are summarized in Table 1. The BET surface area of these oxide precursors is in the range of 22–43 m^2/g. In comparing the BET surface areas of the catalyst prepared by different preparation methods, it was found that the surface area of the catalyst prepared by microemulsion method was larger than that of the conventional catalyst. The pore volume of these oxide precursors decreased in a similar order to that observed for the surface area. The average pore diameter of these precursors showed an opposite trend. Table 1 also shows the H_2 chemisorption uptakes of the catalysts. As shown in Table 1, the H_2 adsorption was increased from 8.3×10^{-2} to 10.1×10^{-2} mmol H_2/mmol Fe, by lessening of the catalyst crystal size from conventional to nano-catalyst. A complete characterization of catalysts was presented in our previous work [25,30]. These results indicate that the crystal size of nano and conventional catalysts is about 20 nm and 0.6 μm, respectively.

Table 1. N_2 adsorption at 77 K and H_2 uptake on reduced catalysts

Catalysts	BET surface area (m^2/g)	Pore volume^a (cm^3/g)	Average pore diameter^a (nm)	H_2 uptake^b ($\times 10^{-2}$ mmol H_2/mmol Fe)
Conventional	22	0.15	21.6	8.3
Nano catalyst	43	0.31	14.6	10.1

^{a}These values were calculated by BHJ method from desorption isotherm.
^{b}The H_2 uptake on catalysts was determined by calculating the area under the H_2-TPD curves, until H_2 disappeared in effluent of reactor

5.2. Studies on product distributions

The chain length distribution of Fischer-Tropsch products formed on the iron catalyst can be well characterized by a two ASF distribution. Our results focus on the effect of process variables and iron crystal size on carbon number distribution. In all cases, a double α-ASF distribution was required to fit the data. Chain length distributions were calculated using a method described by Donnelly et al. [22] as described in previous section. Typically we used the entire range from C_3 to C_{22} to calculate α_1 and α_2. The chain length distributions and growth probabilities α_1 and α_2 depend mainly on reaction conditions of the FT synthesis and catalysts crystal size.

The effects of H_2/CO partial pressure ratios on chain length distribution at 563 K, 1.7 MPa, and space velocity 4.9 nl·h^{-1}·g$_{Fe}^{-1}$ for conventional and nanosize iron catalysts are given in Figures 1 and 2, respectively. These Figures show that the average carbon number of products is decreased with increasing the H_2/CO partial pressures ratios and/or decreas-
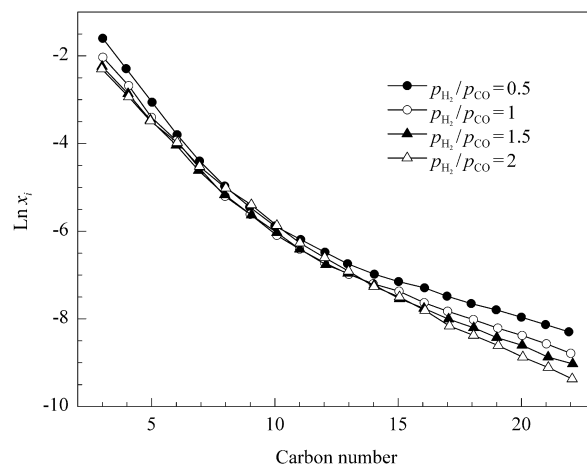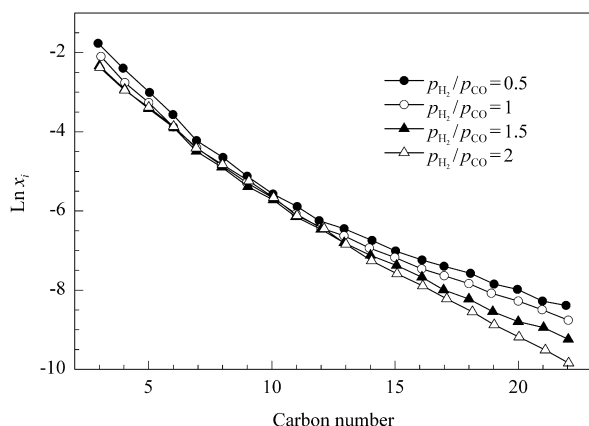

Figure 1. The effects of H_2/CO partial pressure ratios in feed on chain length products distribution of Fe/Cu/La conventional catalyst. Reaction conditions: 563 K, total pressure 1.7 MPa, and space velocity 4.9 nl·h^{-1}·g$_{Fe}^{-1}$

ing the iron crystal size from conventional to nano catalyst. As shown in Figures 1 and 2, with increasing the H$_2$/CO partial pressure ratios and/or decreasing the catalyst crystal size, deviation from normal ASF distribution decreases and a double-α-ASF distribution changes into a straight line.

Chain length products distributions for conventional and nano catalysts, at different reaction temperatures are given in Figures 3 and 4. These Figures show that with increasing the reaction temperatures, average carbon number of products was decreased and break down in ASF distribution decreased.

Figure 2. The effects of H$_2$/CO partial pressures ratios in feed on chain length products distribution of Fe/Cu/La nano catalyst. Reaction conditions: 563 K, total pressure 1.7 MPa, and space velocity 4.9 nl·h^{-1}·g$_{Fe}^{-1}$
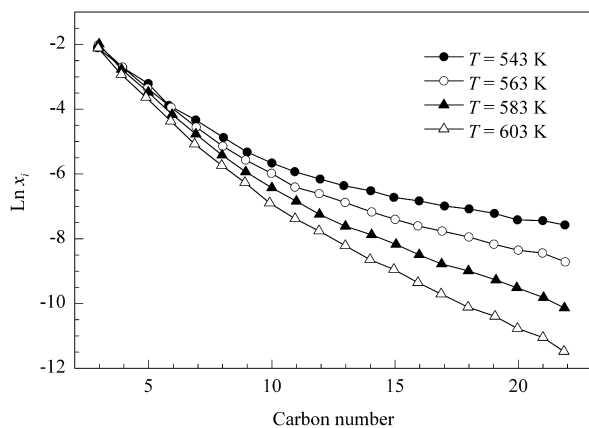

Figure 3. Effects of reaction temperatures on chain length products distributions of Fe/Cu/La conventional catalyst. Reaction conditions: $P_{H_2}/P_{CO} = 1$, 1.7 MPa, and space velocity 4.9 nl·h^{-1}·g$_{Fe}^{-1}$

The characterizing growth probabilities α_1 and α_2 for two catalysts are listed in Table 2. These results indicated that both probabilities are depending on reaction conditions and catalyst crystal size. Table 2 illustrates that the value of α_1 is slightly increased while the growth probability α_2 is slightly decreased as the H$_2$/CO mole ratio is raised and/or iron crystal size is decreased. Also the values of α_1 and α_2 are slightly decreased, as the temperature is increased. A similar result is obtained by Donnelly and Satterfield [33] and Dictor and Bell [13]. These results indicated that by increasing the reaction temperature, breaks down in ASF distribution decreases.
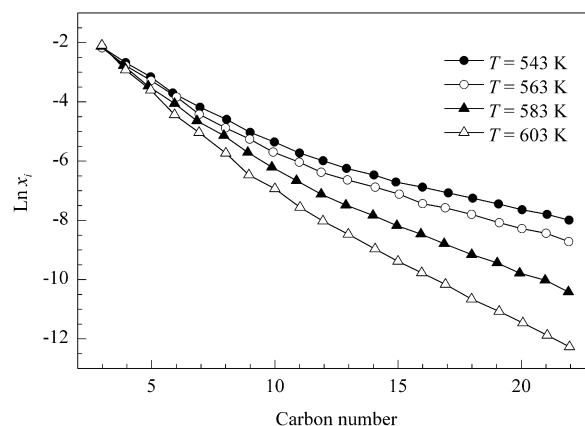

Figure 4. Effects of reaction temperatures on chain length products distributions of Fe/Cu/La nano catalyst. Reaction conditions: $P_{H_2}/P_{CO} = 1$, 1.7 MPa, and space velocity 4.9 nl·h^{-1}·g$_{Fe}^{-1}$

Table 2. Chain growth probabilities and kinetics parameters of FTS reactions for conventional and nano catalysts

		Conventional catalyst		Nano catalyst	
		α_1	α_2	α_1	α_2
T(K)	543	0.52	0.88	0.55	0.84
	563	0.49	0.83	0.53	0.81
	583	0.47	0.77	0.50	0.74
	603	0.45	0.71	0.44	0.67
P_{H_2}/P_{CO}	0.5	0.47	0.85	0.51	0.82
	1	0.49	0.83	0.53	0.81
	1.5	0.51	0.81	0.55	0.78
	2	0.54	0.78	0.57	0.74
A_t/A_p		15	8.8×10^3	59	3.2×10^3
$E_p - E_t$ (kJ/mol)		−12.6	−50	−19.5	−41

5.3. Kinetics studies

Figures 5 and 6 show that the experimentally observed values of chain growth probabilities α_1 and α_2 produce a straight line when $(1-\alpha)/\alpha$ is plotted versus P_{H_2}/P_{CO} for conventional and nano catalysts. For conventional Fe/Cu/La catalyst, based on the equations of the straight line for the experimentally results of Figure 5, the obtained equations of the chain growth probabilities α_1 and α_2 as function of P_{H_2}/P_{CO} are:

$$\alpha_1 = \frac{1}{2.2 - 0.18\dfrac{P_{H_2}}{P_{CO}}} \tag{16}$$

$$\alpha_2 = \frac{1}{1.14 - 0.069\dfrac{P_{H_2}}{P_{CO}}} \tag{17}$$

Similarly, for nano-size Fe/Cu/La catalyst, the obtained equations of the chain growth probabilities α_1 and α_2 as function of P_{H_2}/P_{CO} are:

$$\alpha_1 = \frac{1}{2.03 - 0.14\dfrac{P_{H_2}}{P_{CO}}} \tag{18}$$

$$\alpha_2 = \frac{1}{1.16 - 0.089\dfrac{P_{H_2}}{P_{CO}}} \tag{19}$$
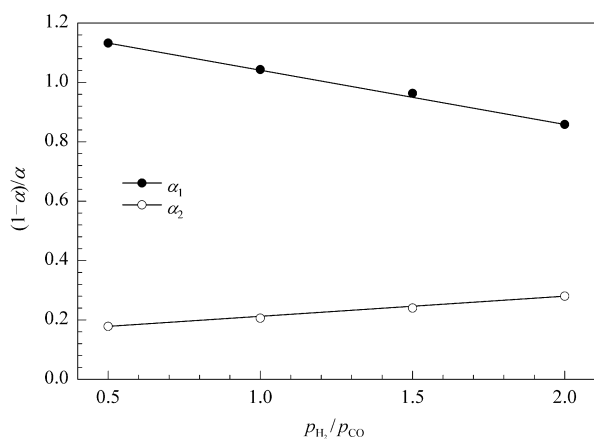

Figure 5. Empirical correlation between growth probabilities α_1, α_2 and reactant partial pressures for Fe/Cu/La conventional catalyst. Reaction conditions: 563 K, total pressure1.7 MPa, and space velocity 4.9 nl·h^{-1}·g$_{Fe}^{-1}$
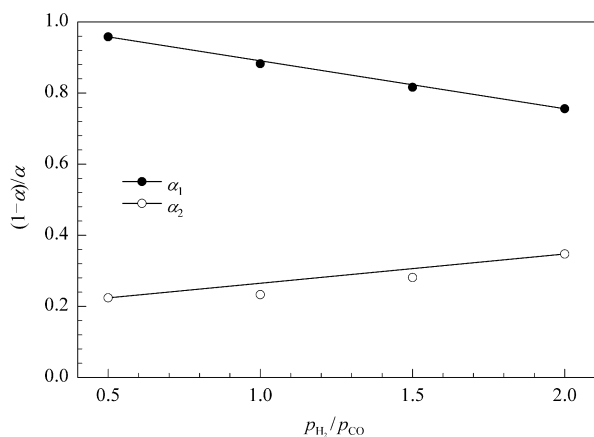
Figure 6. Empirical correlation between growth probabilities α_1, α_2 and reactant partial pressures for Fe/Cu/La nano catalyst. Reaction conditions: 563 K, total pressure1.7 MPa, and space velocity 4.9 nl·h^{-1}·g$_{Fe}^{-1}$

These equations show that the dependence of α on H$_2$ and CO partial pressures for α_2 is much weaker than α_1 for both catalysts. Also, dependence of α_1 on H$_2$ and CO partial pressures for conventional catalyst was higher and this relation for α_2 was on the contrary.

The molar rates of production for C$_3$ and C$_{10}$ hydrocarbons as a function of P_{H_2} and P_{CO} in the form of power-law rate expressions for conventional Fe/Cu/La catalyst, by fitting the experimentally results were obtained as:

$$R_{C_3} = 0.011P_{H_2}^{0.7}P_{CO}^{-0.9} \tag{20}$$

$$R_{C_{10}} = 3 \times 10^{-5}P_{H_2}^{1.7}P_{CO}^{-1.1} \tag{21}$$

Similarly, the molar rates of production for C$_3$ and C$_{10}$ hydrocarbons as a function of P_{H_2} and P_{CO} for Fe/Cu/La nano-catalyst were obtained as:

$$R_{C_3} = 0.025P_{H_2}^{0.1}P_{CO}^{-0.8} \tag{22}$$

$$R_{C_{10}} = 5 \times 10^{-5}P_{H_2}^{1.8}P_{CO}^{-1.1} \tag{23}$$

Based on Dictor and Bell methods for hydrocarbons production rates (Eq. (10)) [13], the hydrocarbons production rates of $i = 4$ to 9 and $i = 11$ to 22 carbon numbers, for Fe/Cu/La conventional catalyst were obtained by combination of Eqs. (20) and (21) with chain growth probabilities α_1 and α_2 as function of P_{H_2}/P_{CO} (Eqs.(16) an (17)), as:

$$R_{C_i} = \frac{0.011P_{H_2}^{0.7}P_{CO}^{-0.9}}{\left(2.2 - 0.18\dfrac{P_{H_2}}{P_{CO}}\right)^{i-1}}, \quad \text{for } i = 4 \text{ to } 9 \tag{24}$$

$$R_{C_i} = \frac{3 \times 10^{-5}P_{H_2}^{1.7}P_{CO}^{-1.1}}{\left(1.14 - 0.069\dfrac{P_{H_2}}{P_{CO}}\right)^{i-1}}, \quad \text{for } i = 11 \text{ to } 22 \tag{25}$$

The observed H$_2$ dependency of light hydrocarbons ($i = 4$ to 9) production was 0.7 and increased with increasing carbon number to 1.7 for heavy ($i = 11$ to 22) hydrocarbons. The observed CO dependency was -0.9 for light hydrocarbons ($i = 4$ to 9) and decreased slightly with increasing carbon number. Similarly, the hydrocarbons production rates with $i = 4$ to 9 and $i = 11$ to 22 carbon numbers, for Fe/Cu/La nano catalyst were obtained by combination of Eqs. (22) and (23) with Eqs. (18) and (19) as:

$$R_{C_i} = \frac{0.025P_{H_2}^{0.1}P_{CO}^{-0.8}}{\left(2.03 - 0.14\dfrac{P_{H_2}}{P_{CO}}\right)^{i-1}}, \quad \text{for } i = 4 \text{ to } 9 \tag{26}$$

$$R_{C_i} = \frac{5 \times 10^{-5}P_{H_2}^{1.8}P_{CO}^{-1.1}}{\left(1.16 - 0.089\dfrac{P_{H_2}}{P_{CO}}\right)^{i-1}}, \quad \text{for } i = 11 \text{ to } 22 \tag{27}$$

The calculated and experimental results are shown in Figures 7 to 10 for conventional and nano catalysts. These Figures show that the experimental data are almost in agreement with the calculated results and indicated similar trends for both catalysts. Dictor and Bell [13] reported that the kinetics of formation of product by considering Eq. (10), formation of methane as R_{C_1} and considering of normal ASF with one chain growth, cannot be represented by simple power-law rate expression. But the present work shows that a useful simple power-law rate expression can be produced by considering a double-α-ASF distribution. The curvature seen in the lines is a direct result of the dependence of α on the reactant partial pressures and the dependence of R_{C_i} on α^{i-1}. Since the dependence of α on H$_2$ and CO partial pressures for α_2 is much weaker than α_1 for both catalysts the kinetics for C$_{11}$–C$_{22}$ hydrocarbon synthesis is dominated by the power-law dependence of $R_{C_{10}}$.
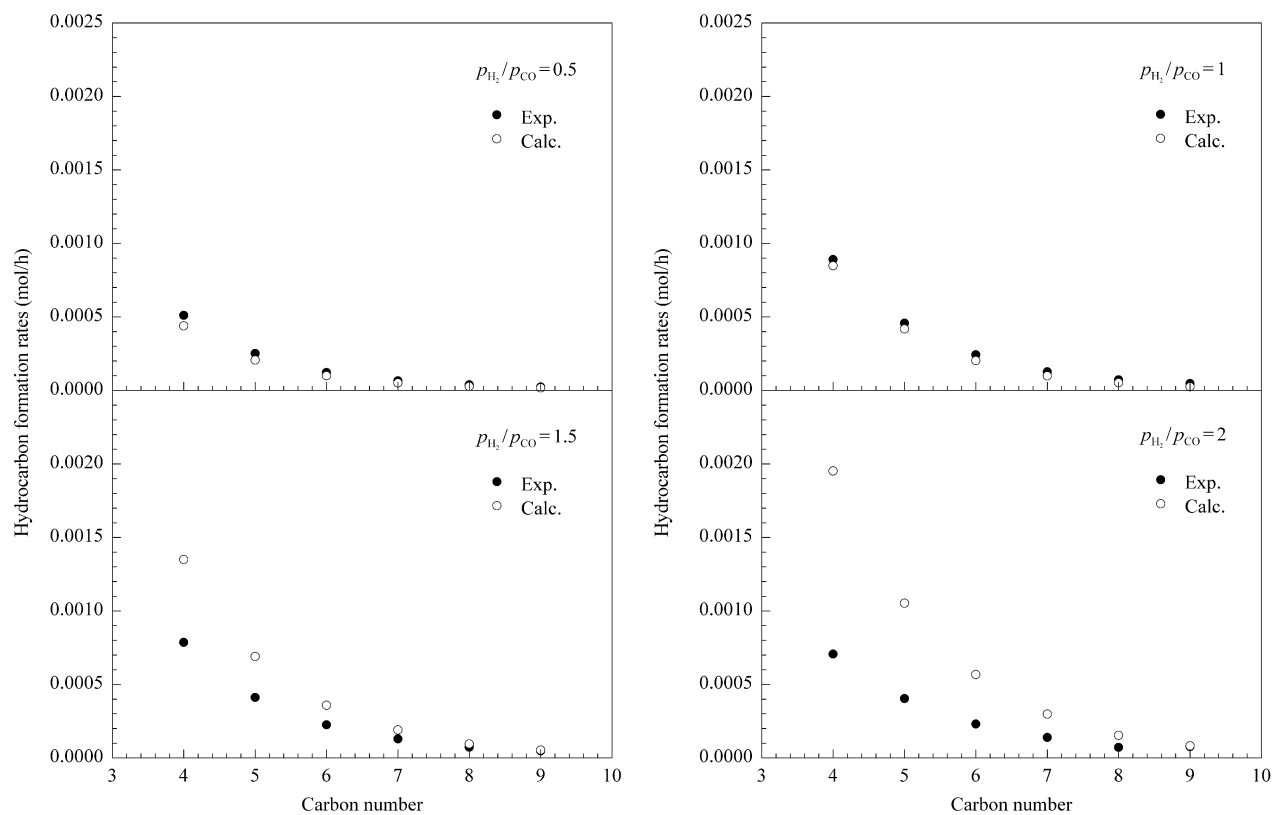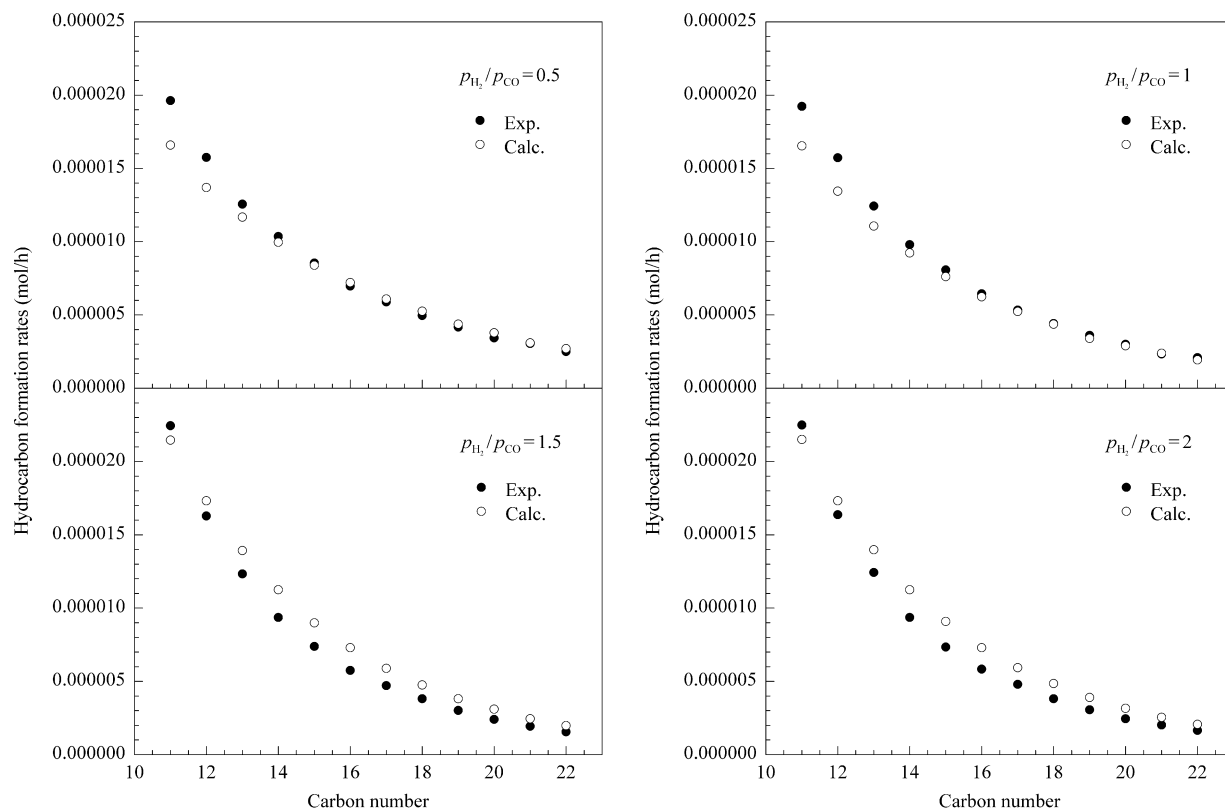
Figure 7. Comparison between experimental results for $i = 4$ to 9 carbon products formation rates and calculated results by considering of chain length probability α_1 for Fe/Cu/La conventional catalyst. Reaction conditions: 563 K, 1.7 MPa, and space velocity, 4.9 nl·h^{-1}·g$_{Fe}^{-1}$

Figure 8. Comparison between experimental results for $i = 11$ to 22 carbon products formation rates and calculated results by considering of chain length probability α_2 for Fe/Cu/La conventional catalyst. Reaction conditions: 563 K, 1.7 MPa, and space velocity, 4.9 nl·h^{-1}·g$_{Fe}^{-1}$
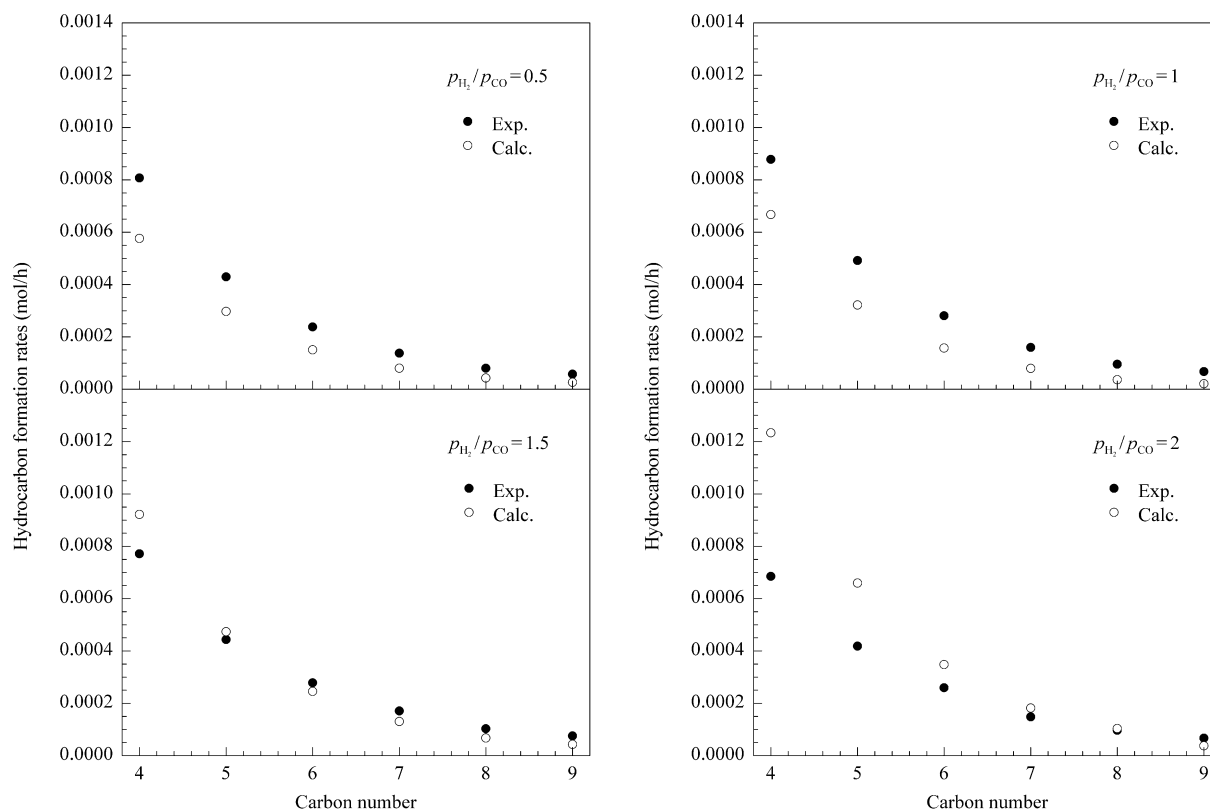
Figure 9. Comparison between experimental results for $i = 4$ to 9 carbons product formation rates and calculated results by considering of chain length probability α_1 for Fe/Cu/La nano catalyst. Reaction conditions: 563 K, 1.7 MPa, and space velocity, 4.9 nl·h^{-1}·g$_{Fe}^{-1}$
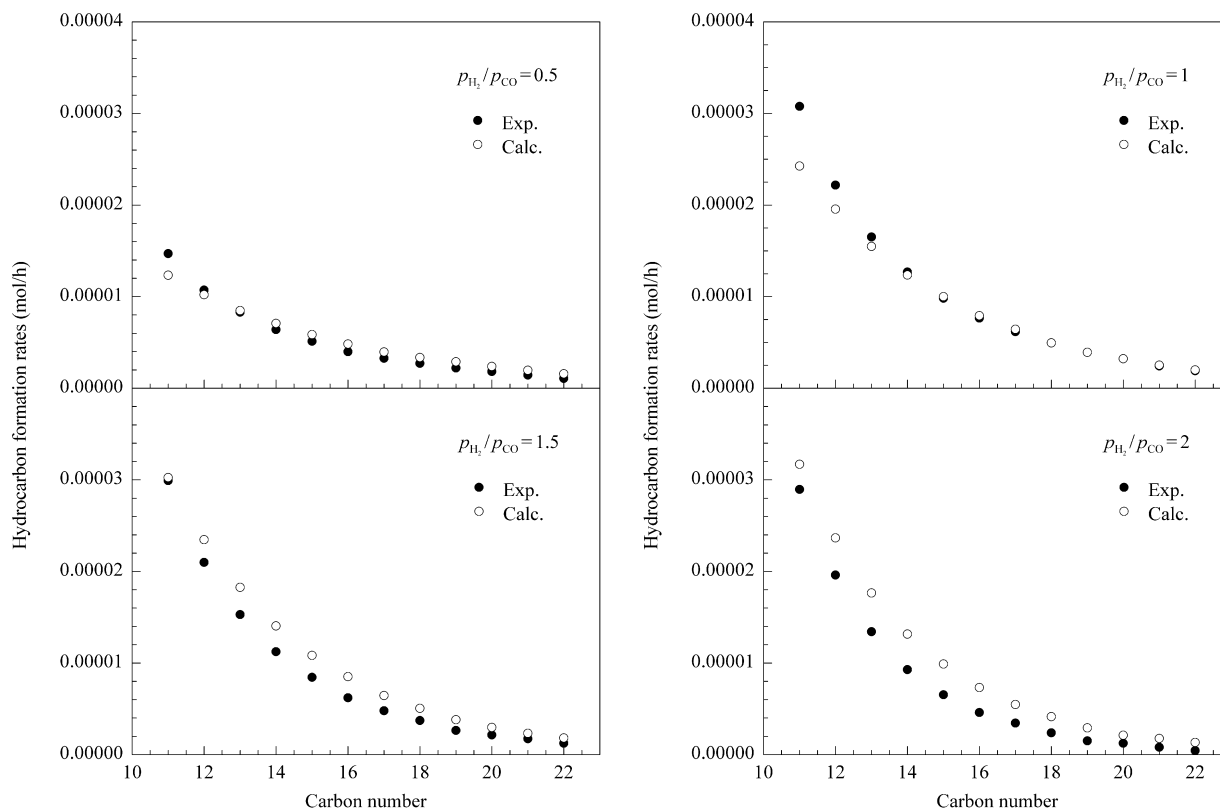

Figure 10. Comparison between experimental results for $i = 11$ to 22 carbons product formation rates and calculated results by considering of chain length probability α_2 for Fe/Cu/La nano catalyst. Reaction conditions: 563 K, 1.7 MPa, and space velocity, 4.9 nl·h^{-1}·g$_{Fe}^{-1}$

The plots of $\ln[(1-\alpha)/\alpha]$ versus $1/T$ for evaluation of temperature dependency of chain growth probabilities α_1 and α_2 for conventional and nano Fe/Cu/La catalysts, are shown in Figures 11 and 12, respectively. Table 2 indicated the chain growth probabilities α_1 and α_2 are highly dependent on the reaction temperature, and decreases with increasing reaction temperature. From the slopes and the intercepts of the straight lines in Figures 11 and 12, the difference between activation energies for propagation and termination reactions ($E_p - E_t$) and the ratio A_t/A_p are obtained (listed in Table 2). As shown in Table 2, the reaction activation barrier of the chain growth is lower than that of the chain termination for both α_1 and α_2 growth probabilities, but $E_p - E_t$ difference for α_1 is lower than α_2. This may be due to the fact that the mechanisms of chain growth probabilities α_1 and α_2 are incompatible for the activation energies because of differences in mechanisms for chain growth and termination. As shown in Table 2, by decreasing the catalyst crystal size from conventional to nano scale, the difference $E_p - E_t$ calculated from α_1 increased but for α_2 decreased.
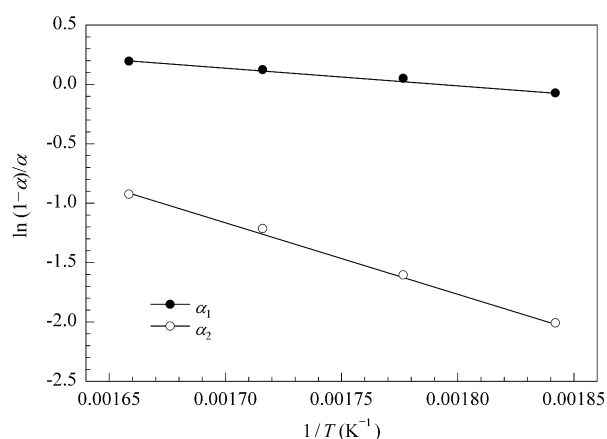

Figure 11. Empirical correlation between growth probabilities α_1, α_2 and reciprocal reaction temperatures for Fe/Cu/La conventional catalyst. Reaction conditions: $P_{H_2}/P_{CO} = 1$, 1.7 MPa, and space velocity, 4.9 nl·h^{-1}·g$_{Fe}^{-1}$
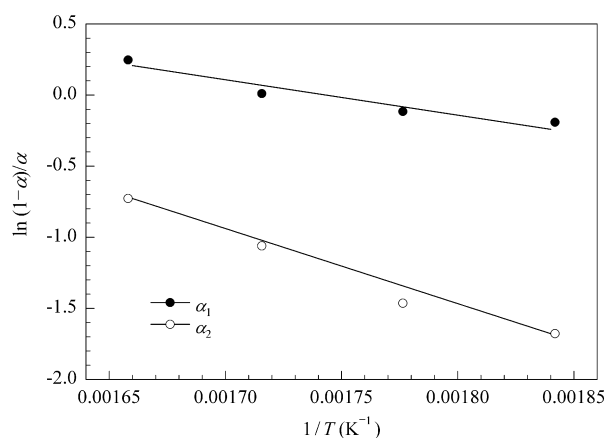

Figure 12. Empirical correlation between growth probabilities α_1, α_2 and reciprocal reaction temperatures for Fe/Cu/La nano catalyst. Reaction conditions: $P_{H_2}/P_{CO} = 1$, total pressure 1.7 MPa, and space velocity 4.9 nl·h^{-1}·g$_{Fe}^{-1}$

6. Discussion

In this experiment, the hydrocarbon production rates and carbon number distribution of conventional and nano-size lanthanum promoted iron catalysts in Fischer-Tropsch synthesis were studied. The concept of Anderson-Schulz-Flory (ASF) distribution with two chain growth probabilities was used for evaluation of experimental data. This method proposed by Donnelly et al. [22] was used to characterize the carbon number distribution of Fischer-Tropsch synthesis where independent ASF distributions with different chain growth probabilities are superimposed. The carbon number distribution of the products formed on iron catalysts can be represented by two ASF distributions with its break shown on C_{10} in Figures 1 to 4. These results show that when the iron crystal size decreased from conventional to nano catalysts, the average carbon number of products was decreased and the break in the product distribution curve was less observed. The origin of the break is not established clearly. König and Gaube [18] and Satterfield and Hff [16] proposed that the two branches observed with potassium promoted iron catalysts are due to the synthesis over two groups of active sites differing in their promotion level. This interpretation may not be the only one, since Huff and Satterfield [6] have shown that some unpromoted iron catalysts can also produce ASF plots, which consist of two branches. Dictor and Bell [13] suggested generally that deviations from uniform ASF distributions might result from the chemistry of the synthesis. The most accepted mechanism is CH_2 insertion, which leads to conclude the carbide theory of Fischer-Tropsch [37]. In this mechanism, chain termination occurs mainly with hydrogen β-elimination and 1-alkenes being desorbed as primary products. In the following reactions, readsorbed 1-alkenes are hydrogenated to form intermediates for surface intermediates chain growth with C_1 surface species. These C_1 species having various hydrogenation degrees are the following: CO, HCO, HCOH, CH, and CH_2.

Patzlaff et al. [23] have discussed the distribution which is characterized with α_1 is built up by monomers that exhibited higher degree of hydrogenation than those attributed with α_2. Therefore, CH_2 is assumed as C_1 intermediate attributed to the distribution of growth probability α_1. Obviously, hydrocarbon chains growth probability α_2 is built up due to monomers except CH_2 species with lower degree of hydrogenation. Higher hydrogen concentration on catalyst surface enhanced the concentration of monomers with higher degree of hydrogenation and increased the α_1 chain growth probability. As a result, the products with higher carbon number and related chain growth probability (α_2) are decreased by increasing the H_2 partial pressures. Figures 1 and 2 showed that by increasing the H_2/CO ratio, the average carbon number in products decreased. Also, Table 2 shows that the growth probability α_1 is increased, while growth probability α_2 is decreased by increasing the H_2/CO partial pressures ratio. Although at higher hydrogen partial pressures α_1 and α_2 growth probabilities are close together and break down of the ASF distribution decreased. Results of Table 2, Figures 1 and 2 show that by decreasing the catalyst crystal size from conventional to nano scale, chain length distributions and α_2 chain growth probability decreased while α_1 chain growth probabil-

ity increased. This fact can be interpreted by higher surface and higher amounts of H_2 adsorbed on nano-catalyst (see Table 1). As represented in Table 1 by decreasing the catalyst crystal size, the concentration of H_2 on the surface of catalyst was increased and the concentration of monomers with higher degree of hydrogenation was enhanced and therefore, the α_1 chain growth probability was increased.

Table 2 and Figures 3 to 4 indicated that by increasing the FTS reaction temperatures, the heavier products formation rates and values of α_1 and α_2 are slightly decreased. This fact may be related to elevated mobility of hydrocarbons chains on the surface of catalysts at the high temperature that increased the vibrations of growing chains on catalyst surface and caused the hydrocarbons to be desorbed more quickly. As a result, average carbon number and both chain growth probabilities α_1 and α_2 decrease at higher temperatures.

Table 2 predicted that the reaction activation barrier of the chain growth is lower than that of chain termination ($E_p - E_t$) for both α_1 and α_2 chain growth probabilities. Also, $E_p - E_t$ difference for α_1 is lower than α_2 chain growth probability. This may be due to the fact that the mechanisms of chain growth probabilities α_1 and α_2 are incompatible for the barriers of the chain growth and termination. As described previously, chain growth probability α_1 is attributed to propagation of chain by C_1 intermediate with higher degree of hydrogenation (CH_2, or CH) that have lower activation energies. In contrast, chain growth probability α_2 is attributed to propagation of chain by C_1 intermediate with lower degree of hydrogenation (CO, HCO, HCOH, CH) that have higher activation energies. As shown in Table 2, by decreasing the catalyst crystal size from conventional to nano scale, the difference $E_p - E_t$ for α_1 increased but for α_2 decreased, because of higher concentration of adsorbed H_2 on the surface of catalyst which increased the concentration of C_1 intermediate with higher degree of hydrogenation and decreased the C_1 intermediate with lower degree of hydrogenation.

7. Conclusions

Studies on chain length distributions of Fischer-Tropsch products have led to the assumptions of two distinctive mechanism of chain growth that cause a superposition of two ASF distributions. The concept of two superimposed Anderson-Schulz-Flory (ASF) distributions has been applied for the representation of the effects of reaction conditions and nano-size particles on kinetics parameters and product distributions.

These results indicated that both probabilities α_1 and α_2 are depended on reaction conditions and catalyst crystal size. The value of α_1 is slightly increased while the growth probability α_2 is slightly decreased as the H_2/CO mole ratio is raised and/or iron crystal size is decreased. Also the values of α_1 and α_2 are slightly decreased, as the temperature is increased. This fact reveals the chain growth probabilities α_1 and α_2 have different mechanisms for chain growth and termination. The chain growth probability α_1 is attributed to propagation of chain by C_1 intermediate with higher degree of hydrogenation (CH_2, or CH) that have lower activation energies. In contrast, chain growth probability α_2 is attributed to propagation of chain by C_1 intermediate with lower degree of hydrogenation (CO, HCO, HCOH, CH) that have higher activation energies.

These results reveal that by reducing the particle size of catalyst, the break in ASF distributions was decreased. Also useful different kinetics equations for synthesis of C_3 to C_9 and C_{10} to C_{22} were determined by using α_1 and α_2 chain growth probabilities.

References

[1] Anderson R B. The Fischer-Tropsch Synthesis. Orlando, FL: Academic Press, 1984
[2] Dry M E. The Fischer-Tropsch Synthesis. In: Anderson J R, Boudart M, Ed. Catalysis: Science and Technology, vol 1. Berlin; New York: Springer-Verlag, 1981, 159
[3] Bartholomew C H. *Stud Surf Sci Catal*, 1991, Vol 64, 158
[4] Herington E F G. *Chem Ind* (*London*), 1946, (38): 346
[5] Friedel R A, Anderson R B. *J Am Chem Soc*, 1950, 72(3): 1212
[6] Huff G A, Satterfield C N. *Ind Eng Chem*, *Process Des Dev*, 1985, 24(4): 986
[7] Wojciechowski B W. *Catal Rev-Sci Eng*, 1988, 30(4): 629
[8] Novak S, Madon R J, Suhl H. *J Chem Phys*, 1981, 74(11): 6083
[9] Novak S, Madon R J, Suhl H. *J Catal*, 1982, 77(1): 141
[10] Iglesia E, Soled S L, Baumgartner J E, Reyes S C. *J Catal*, 1995, 153(1): 108
[11] Pichler H, Schulz H, Elstner M. *Brennst Chem*. 1967, 48(3): 78
[12] Dry M E. *J Mol Catal*, 1982, 17(2-3): 133
[13] Dictor R A, Bell A T. *J Catal*, 1986, 97(1): 121
[14] Puskas I, Hurlbut R S. *Catal Today*, 2003, 84(1-2): 99
[15] Puskas I, Hurlbut R S, Pauls R E. *J Catal*, 1993, 139(2): 591
[16] Satterfield C N, Huff G A. *J Catal*, 1982, 73(1): 187
[17] Madon R J, Taylor W F. *J Catal*, 1981, 69(1): 32
[18] König L, Gaube J. *Chem Ing Tech*, 1983, 55(1): 14
[19] Schliebs B, Gaube J. *Ber Bunsen-ges Phys Chem*, 1985, 89: 68
[20] Satterfield C N, Huff G A, Longwell J P. *Ind Eng Chem*, *Process Des Dev*, 1982, 21(3): 465
[21] Huff G A, Satterfield C N. *J Catal*, 1984, 85(2): 370
[22] Donnelly T J, Yates I C, Satterfield C N. *Energy Fuels*, 1988, 2(6): 734
[23] Patzlaff J, Liu Y, Graffmann C, Gaube J. *Appl Catal A*, 1999, 186(1-2): 109
[24] Pour A N, Zamani Y, Tavasoli A, Shahri S M K, Taheri S A. *Fuel*, 2008, 87(10-11): 2004
[25] Pour A N, Shahri S M K, Bozorgzadeh H R, Zamani Y, Tavasoli A, Marvast M A. *Appl Catal A*, 2008, 348(2): 201
[26] Pour A N, Zare M, Zamani Y. *J Natur Gas Chem*, 2010, 19: 31
[27] Pour A N, Shahri S M K, Zamani Y, Irani M, Tehrani S. *J Natur Gas Chem*, 2008, 17: 24
[28] Pour A N, Zare M,Shahri SMK, Zamani Y, Alaei M R. *J Natur Gas Sc Eng*, 2009, 1: 183
[29] Sarkar A, Seth D, Dozier A K, Neathery J K, Hamdeh H H, Davis B H. *Catal Lett*, 2007, 117(1-2): 1
[30] Pour A N, Taghipoor S, Shekarriz M, Shahri S M K, Zamani Y. *J Nanosci Nanotech*, 2009, 9(7): 4425
[31] Herranz T, Rojas S, Perez-Alonso F J, Ojeda M, Terreros P, Fierro J L G. *Appl Catal A*, 2006, 311: 66
[32] Eriksson S, Nylen U, Rojas S, Boutonnet M. *Appl Catal A*, 2004, 265(2): 207
[33] Schwuger M J, Stickdorn K, Schomacker R. *Chem Rev*, 1995, 95(4): 849
[34] Van der Laan G P, Beenackers A A C M. *Catal Rev-Sci Eng*, 1999, 41(3-4): 255
[35] Yang Y N, Pen S Y, Zhong B, Wang Q. *Catal lett*, 1993, 19: 93
[36] Donnelly T J, Satterfield C N. *Appl Catal*, 1989, 52(1-2): 93
[37] Fischer F, Tropsch H. *Brennst Chem*, 1926, 7: 97